

Article

# X-ray Photoelectron Spectroscopy (XPS) Study of the Products Formed on Sulfide Minerals Upon the Interaction with Aqueous Platinum (IV) Chloride Complexes

Alexander Romanchenko , Maxim Likhatski and Yuri Mikhlin 

Institute of Chemistry and Chemical Technology, Siberian Branch of the Russian Academy of Sciences, Krasnoyarsk 660036, Russia; lixmax@icct.ru (M.L.); yumikh@icct.ru (Y.M.)

\* Correspondence: romaas82@mail.ru; Tel.: +7-391-205-1928

Received: 8 November 2018; Accepted: 6 December 2018; Published: 8 December 2018



**Abstract:** The interaction of aqueous solutions bearing platinum-group elements (PGEs) with sulfides is important for understanding the formation and weathering of PGE ore deposits, mineral processing, and synthesis of nanomaterials. Here, the surface species formed upon the contact of the main sulfide minerals (pyrite, pyrrhotite, galena, chalcopyrite and valleriite) with the solutions of  $H_2PtCl_6$  (pH 1.5, 20 °C) have been studied using X-ray photoelectron spectroscopy (XPS). Uptake of Pt increased gradually with increasing interaction time, and depended, as well as the composition of immobilized products, on the mineral nature and the state of its surface, e.g., the chemical pre-treatment. The highest rate of Pt deposition was observed on galena and valleriite and the lowest on pyrite and pyrrhotite. The preliminary moderate oxidation of pyrrhotite promoted Pt deposition, which, however, was hindered under harsh reaction conditions. The pre-oxidation of pyrite in all cases resulted in a decrease of the Pt deposition. Initially, Pt(IV) chloride complexes adsorb onto the mineral surface, and then the reduction of Pt(IV) to Pt(II) and substitution of chloride ions with sulfide groups occur forming sulfides of Pt(II) and then, Pt(IV). The reduction of Pt species to the metallic state was observed at valleriite after 24 h, probably due the negative charge of the sulfide nanolayers of this sulfide-hydroxide composite mineral.

**Keywords:** XPS; sulfide minerals; platinum; deposition; valleriite; chloride complexes

## 1. Introduction

Platinum-group elements (PGEs) are widely used in various areas, first of all in catalysis; their chalcogenides are also of interest for electrocatalysis [1–3]. The increasing industrial demand for PGEs and their limited natural sources require the investigation of the genesis of PGE ores and new approaches to the recovery technologies [4], secondary processes and environmental behavior of engineered PGE species [5,6]. Platinum-group element ores are mainly associated with ultramafic-mafic rocks and, little is known about the interaction of Pt-bearing aqueous solutions with sulfide minerals [7–20]. Platinum-group element deposits of hydrothermal origin exist, and mechanisms of hydrothermal transportation of PGEs [9–12], including the biological transport and transformation [21–24] have been studied since the end of the 1980s.

Platinum-group elements are commonly associated with base metal sulfides, particularly pentlandite, pyrrhotite, chalcopyrite, pyrite [15,25,26]. Palladium is hosted in base metal sulfides (mainly pentlandite) and occurs both within the crystal lattice and as nanometer-sized inclusions of discrete PGE minerals [27]. Platinum usually has low concentrations within base metal sulfides and mainly forms discrete platinum-group minerals (PGMs). Most work has been focused on

the experimental study and mathematical modeling of Pt dissolution, and stability of its complex compounds with ligands such as  $\text{HS}^-$ ,  $\text{Cl}^-$ ,  $\text{S}_2\text{O}_3^{2-}$ ,  $\text{OH}^-$ ,  $\text{NH}_3$  [11,12,17,18,22,28,29]. At low temperature conditions, acidic pHs and high redox potential, Pt transport by chloride ions is the most suitable [18,30].

In addition to the understanding of mobilization and deposition of PGEs, the interaction of Pt-bearing solutions with base metal sulfides is important for mineral processing of PGEs by heap leaching [31–37] and concentrator plants [35]. Platinum-group elements transfer into solution by leaching (both under technological and natural conditions) can then be taken up on the surface of sulfide minerals. However, in contrast to the vast literature devoted to the interaction of aqueous solutions of gold and silver with sulfides (see, e.g., [38–40] and references therein), only limited studies describe the deposition of PGEs, on the surface of pyrite, galena and sphalerite by X-ray photoelectron spectroscopy (XPS) [16,41]. By the interaction of the  $\text{Na}_2\text{PdCl}_4$  solution (pH 4) with pyrite, sulfide species of Pd(II) are formed at room temperature along with retaining mixed aqua- and hydrochloride complexes of Pd(II) [16]. Recently [41], the interaction of the acidic solution of  $\text{H}_2\text{PdCl}_4$  solution with pyrrhotite and pyrite before and after their preliminarily leaching under different conditions was studied. Palladium-oxyhydroxides are not formed, though it is not completely proved since the differences in the binding energies of the Pd 3d line of oxides and sulfides are not significant [42,43]. So far, no studies analyzing Pt species immobilized from aqueous solutions onto sulfide minerals, and kinetics of their interaction have been carried out yet.

The aim of this study to investigate the chemical species of Pt formed on the surface of sulfide minerals, including the preliminarily oxidized ones, upon their contact with aqueous Pt(IV)-chloride complexes. This knowledge is important for understanding processes leading to the loss of PGEs in the processing of sulfide ores, affinage, and the behavior of PGEs in tailing ponds where they are leached under near-surface conditions [5,6]. The interaction of metal sulfides with the solutions of Pt-containing complex compounds is of interest for preparation of composite nanomaterials and their potential use in (electro)catalysis, electronics [1–3].

## 2. Materials and Methods

For this study, natural sulfide minerals from Noril'sk are studied, i.e., pyrrhotite,  $[\text{Fe}_9\text{S}_{10}]$ , containing impurities of pentlandite,  $[(\text{Ni},\text{Fe})_9\text{S}_8]$  (up to 3 wt.%) and chalcopyrite,  $[\text{CuFeS}_2]$  (1–2 wt.%), and chalcopyrite. Pyrite,  $[\text{FeS}_2]$ , and galena,  $[\text{PbS}]$ , originated from the Sukhoi Log deposit, and the Sanzheevskoe deposit, respectively. Specimens of valleriite,  $[(\text{CuFeS}_2) \cdot 1.5(\text{Mg},\text{Al})(\text{OH})_2]$  from the Nadezhda deposit (Noril'sk provenance) contained about 50% of the target mineral and varying minor quantities of pyrrhotite, chalcopyrite, magnetite, serpentine, pyrite; in more detail this material was characterized in refs. [39,44–50]. Plates with the size of approximately  $2 \times 4 \times 5$  mm were cut from the minerals, and the surface was polished with sandpaper, washed with distilled water and wiped with wet filter paper to remove fine particles directly before Pt deposition. Further, the sample was conditioned in the solution of 1 mmol/L  $\text{H}_2\text{PtCl}_6$  + 30 mmol/L HCl, pH 1.5, unless otherwise stated, without stirring at 20 °C for a time varying from 1 h to 48 h, then washed with distilled water and transferred into the photoelectron spectrometer chamber. The Pt solutions were prepared by dissolving of crystalline  $\text{H}_2\text{PtCl}_6$  (Dragcvetmet, Moscow, Russia) in a HCl solution. All solutions were prepared using analytical grade reagents and deionized water (Millipore).

For the preliminary oxidation the minerals were prepared in the same manner as for XPS. To oxidize, leaching was made using the solution of 0.25 M  $\text{FeCl}_3$  + 1 M HCl during 30 min at 50 °C, and then, the sample was rinsed with the solution of 1 M HCl to remove Fe ions and, consequently, to prevent the formation of the products of Fe(III) hydrolysis. Then, the sample was rinsed with distilled water and placed into the  $\text{H}_2\text{PtCl}_6$  solution for a specified period of time, usually, 2–4 h. The electrochemical oxidation was carried out using an Elins P30 SM potentiostat (Elins, Moscow, Russia) in the 1 M HCl solution at a constant potential over 10 minutes. A Pt wire was used as a counter electrode and a saturated Ag/AgCl electrode was used as the reference electrode;

all potentials are given relative to that. After the electrochemical oxidation the mineral sample was rinsed with distilled water and used further for depositing Pt.

The XPS were acquired using a SPECS spectrometer equipped with a PHOIBOS 150 MCD-9 analyzer (SPECS, Berlin, Germany) at an electron take-off angle of  $90^\circ$  employing monochromatic Mg  $K\alpha$  radiation (1253.6 eV) of an X-ray tube operated at 180 W. The analyzer pass energy was 10 eV for narrow scans, and 20 eV for survey spectra. The C 1s peak at 284.45 eV from hydrocarbon contaminations was used as a reference. The Pt  $4f_{7/2,5/2}$ , S  $2p_{3/2,1/2}$  doublets were fitted, after the subtraction of the Shirley-type background, with the coupled peaks with the Gaussian–Lorentzian peak profiles, the spin–orbit splitting of 3.30 eV and 1.19 eV, and the branching ratios of 0.75 and 0.5, respectively, using the CasaXPS software package (version 2.3.16, Casa Software, Teignmouth, UK). The element concentrations on the surface were determined from the wide scan using the empirical sensitivity coefficients. Some photoelectron spectra were measured at the Russian–German laboratory at the dipole magnet beamline of the synchrotron radiation facility BESSY II (Berlin, Germany). Tapping-mode atomic force microscopy (AFM) studies were conducted using a Solver P-47 multimode scanning probe microscope (Nanotekhnologiya MDT, Moscow, Russia) in air at room temperature. A silicon cantilever with the resonance frequencies of 150–250 kHz was used as a probe.

### 3. Results

#### 3.1. Analysis of the Surface of Pyrite and Pyrrhotite Using X-ray Photoelectron Spectroscopy and Atomic Force Microscopy

The XPS spectra show that both Pt and Cl can be detected on the surface of sulfide minerals after the aqueous media treatment (Figure 1). Typically,  $\text{Cl}^-$  ions are weakly adsorbed on the metal sulfide surface and/or can easily be removed by washing with water [39]. Thus, Cl observed in the spectra largely belongs to adsorbed Pt–Cl complexes.

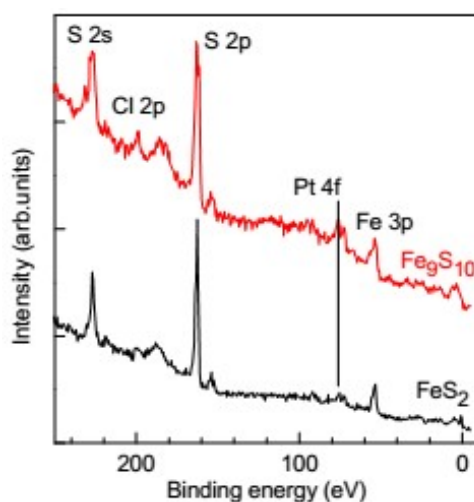


**Figure 1.** Fragments of the X-ray photoelectron survey spectra of pyrite and pyrrhotite after the interaction with 1 mmol/L  $\text{H}_2\text{PtCl}_6$  + 0.03 mol/L HCl solution for 4 h.

Atomic force microscopy (AFM) is used to visualize immobilized Pt products and shows strong changes of the mineral substrate relief due to surface etching. Platinum species are hardly distinguished, especially after the short periods of Pt deposition. Pyrite is a more convenient mineral for the AFM study since its surface is to a lower extent subjected to changes by chemical attack. Figure 2 illustrates regions with the particles of Pt-containing products, in which particles with the lateral size of 50–150 nm cover about 50% of the surface area.

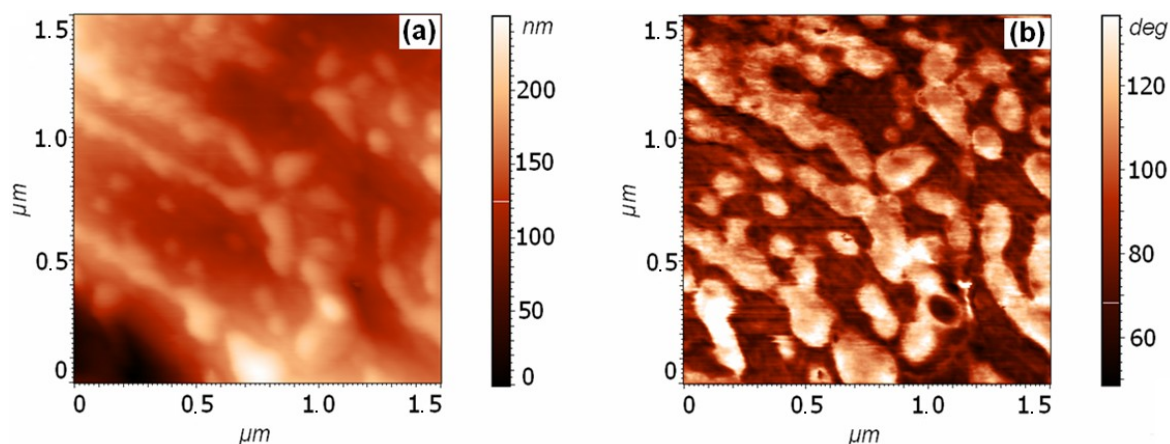


**Figure 2.** Atomic force microscopy images of the pyrite surface after the interaction with the solution of  $H_2PtCl_6$  for 14 h; (a) relief, (b) phase contrast.

### 3.2. Deposition of Platinum Revealed by XPS

#### 3.2.1. Pyrrhotite and Pyrite

Figure 3a,b presents the data on atomic concentrations of Pt, S, Cl, Fe and O on the surface of pyrite and pyrrhotite after the interaction with 1 mmol/L  $H_2PtCl_6$  solutions. The concentrations of Cl and Pt increase with time. The Fe concentration on pyrrhotite gradually decreases with time but it insignificantly changes on pyrite during 24 h.; this is due to various rates of oxidation of these minerals.

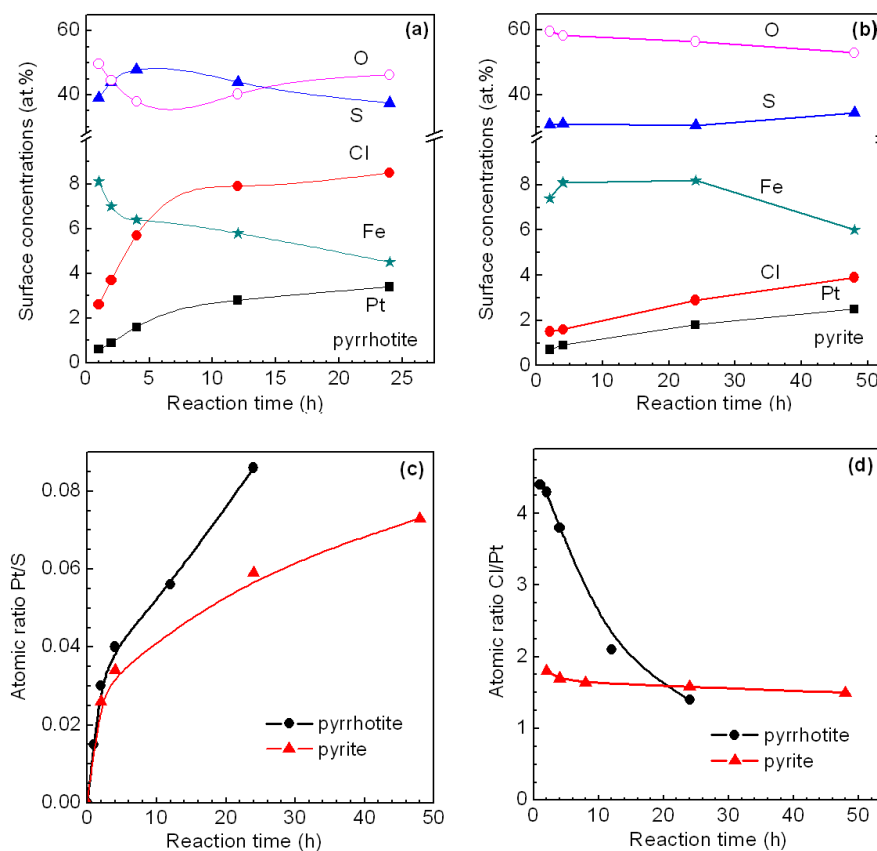


**Figure 3.** Atomic concentrations of Pt, Cl, S, O and Fe on the surface of (a) pyrrhotite and (b) pyrite and the atomic concentration ratios of (c) Pt/S and (d) Cl/Pt on pyrrhotite and pyrite after different interaction time with the  $10^{-3}$  M  $H_2PtCl_6$  solution.

Figure 3c shows that an increase of Pt concentration with time is similar on the surfaces of pyrite and pyrrhotite. The deposition rate is relatively high over 3–5 h, and it gradually decreases but does not drop to zero, so the Pt concentration does not reach saturation. The ratios Cl/Pt show the rate of substitution of Cl<sup>−</sup> ions with sulfide ions and on the influence of this process on the Pt accumulation on the mineral surface. The atomic ratio Cl/Pt is about 1.8 in the initial deposition stage and slightly decreases to 1.5 after 48 h at pyrite. At pyrrhotite, the value of Cl/Pt of approximately 4.3 is apparently higher in the initial stage, and it decreases down to 1.5 over 24 h.

### 3.2.2. Galena, Chalcopyrite and Valleriite

The results of the surface analysis for galena, chalcopyrite and valleriite are presented in Figure 4 and also in Table S1 (Supplementary materials). The deposition of Pt on galena and valleriite is considerably higher than at pyrite and pyrrhotite. The amounts of the Pt normalized to the sulfide phase, that is the ratios Pt/S (Figure 4b), suggest that valleriite accumulates Pt faster than galena and other minerals. The deposition of Pt on chalcopyrite is 1.5 times slower than on galena, while it is 2 times slower on pyrite and pyrrhotite. The Cl/Pt ratios presented in Figure 4c implies a negative correlation between the surface amount of Cl and the accumulation of Pt on the minerals.

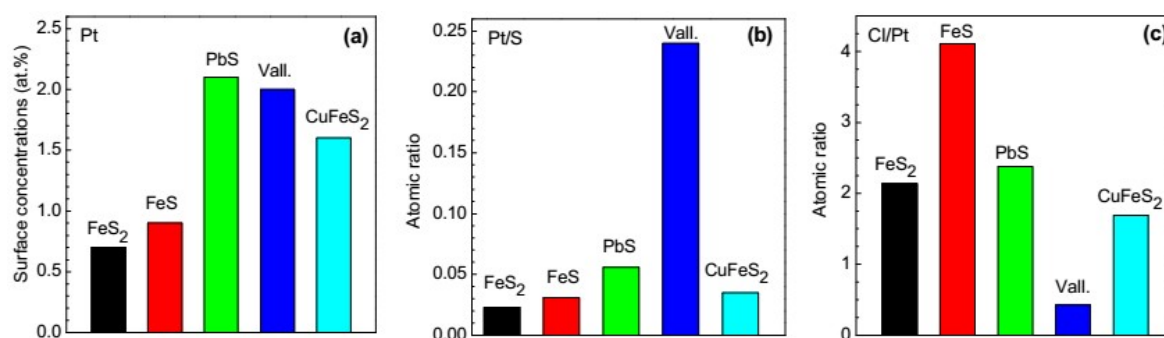


**Figure 4.** Atomic concentrations of (a) Pt, and the ratios (b) Pt/S, and (c) Cl/Pt at the surface of sulfide minerals after 2 h interaction with 1 mmol/L H<sub>2</sub>PtCl<sub>6</sub> solution.

### 3.3. Species of the Deposited Platinum

#### 3.3.1. XPS of the Reference Materials

Photoelectron spectra from reference samples Pt (chloride complexes, Pt sulfide and metallic nanoparticles) precipitated onto highly oriented pyrolytic graphite (HOPG) were preliminarily measured for the reliable assignment of components of Pt 4f spectra. Two components can be revealed in the Pt 4f spectra of pure aqueous H<sub>2</sub>PtCl<sub>6</sub> dried at HOPG, with the component at the binding energy of 72.9 eV being attributable to Pt(II) binding Cl<sup>−</sup> anions, and the high-energy component at 75.0 eV corresponding to PtCl<sub>6</sub><sup>2−</sup> ions (Figure 5a). For the samples of Pt-sulfide hydrosol obtained by mixing the solutions of Na<sub>2</sub>S and H<sub>2</sub>PtCl<sub>6</sub>, two signals with the binding energy of ~74 eV and 72.6 eV can be assigned to Pt(IV)–S and Pt(II)–S compounds [51–53], respectively (Figure 5b). The binding energies can vary in a small range, depending on the S species bound to Pt. Along with minor lines of sulfite and sulfate which are likely to be products of Na<sub>2</sub>S oxidation, two low-energy doublets with S 2p<sub>3/2</sub> at 162.6 eV and 163.3 eV are found in the S 2p spectra (Figure S1, Supplementary materials). These binding energies are typical for disulfide and polysulfide anions, respectively, or other S species carrying similar local negative charges. In its turn, Pt bound with polysulfide could have the binding energy by several tenth eV lower than Pt-sulfide species; this may result in a shift or broadening in the corresponding Pt 4f spectra. The Pt 4f spectra of the metallic Pt particles obtained via the reduction by formaldehyde show the binding energy of Pt<sup>0</sup> metallic nanoparticles to have the value of about 71.5 eV (Figure 5c). The same energy was found for these Pt nanoparticles deposited on pyrite, indicating the absence of the substrate influence on the chemical shift (Figure 5d). The spectra also contain a

minor component from Pt(II)–Cl complexes (73 eV) and a signal at ~72 eV, which is probably due to unidentified product of incomplete reduction of  $\text{H}_2\text{PtCl}_6$ .

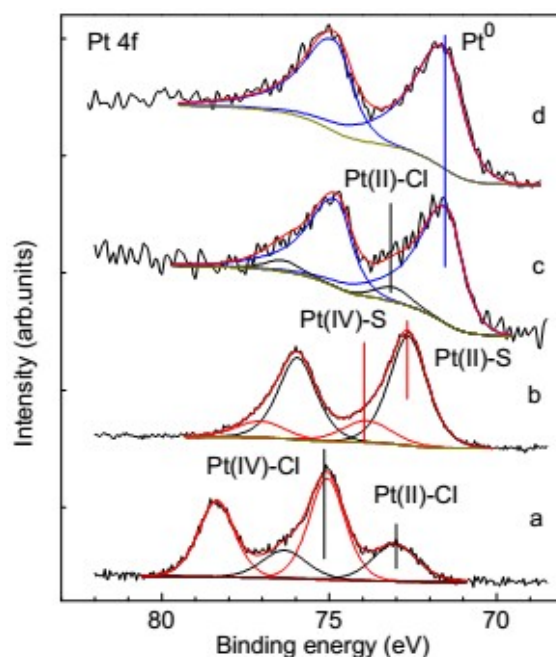


**Figure 5.** X-ray photoelectron spectroscopy (XPS) Pt  $4f_{7/2,5/2}$  spectra from reference Pt compounds deposited on highly oriented pyrolytic graphite (HOPG): (a)  $\text{H}_2\text{PtCl}_6$ , (b)  $\text{H}_2\text{PtCl}_6 + \text{H}_2\text{S}$ , (c) metallic particles, and on pyrite, (d) metallic particles.

### 3.3.2. Change of Platinum Species in the Deposition Process on Pyrite

Figure 6 shows Pt  $4f$  spectra for pyrite interacted with the 1 mmol/L  $\text{H}_2\text{PtCl}_6$  solution. The fitting of the spectra suggests that Pt on the surface is in the form of Pt(II) and Pt(IV) bound both with S and Cl, the proportions of which depending on the deposition duration. The high energy component with the binding energy of 75.2 eV corresponding to the adsorbed complexes of tetravalent Pt is present during the first two hours of the reaction (~25% of total Pt), and then it almost vanishes. Amount of the Pt(IV) species is significantly lower on pyrite than on pyrrhotite (Figures 6 and 7). The share of Pt(II)–Cl species having the binding energy of about 73 eV stays in the range of 30–40%, and thus adsorbed chloride complexes prevail during a 24 h reaction. The Pt  $4f_{7/2}$  component arising afterwards at 74.1 eV can be attributed to Pt(IV) sulfide, possibly  $\text{PtS}_2$  (about 18% of total Pt). The further course of the reaction results in a noticeable decrease of the Pt-chloride species and increase in the amount of Pt(II) sulfide (~72.5 eV). However, the photoelectron spectra acquired using synchrotron radiation with the photon excitation energy of 250 eV (Figure S2, Supplementary materials) having a higher surface sensitivity show slightly different composition of the surface products. The main difference consisting in the presence of the component at 75.0 eV from Pt(IV)–Cl species with the relative intensity up to 8%. Thus, independent of the reaction time, a small amount of the adsorbed  $\text{PtCl}_6^{2-}$  ions seems to be always present on the mineral surfaces.

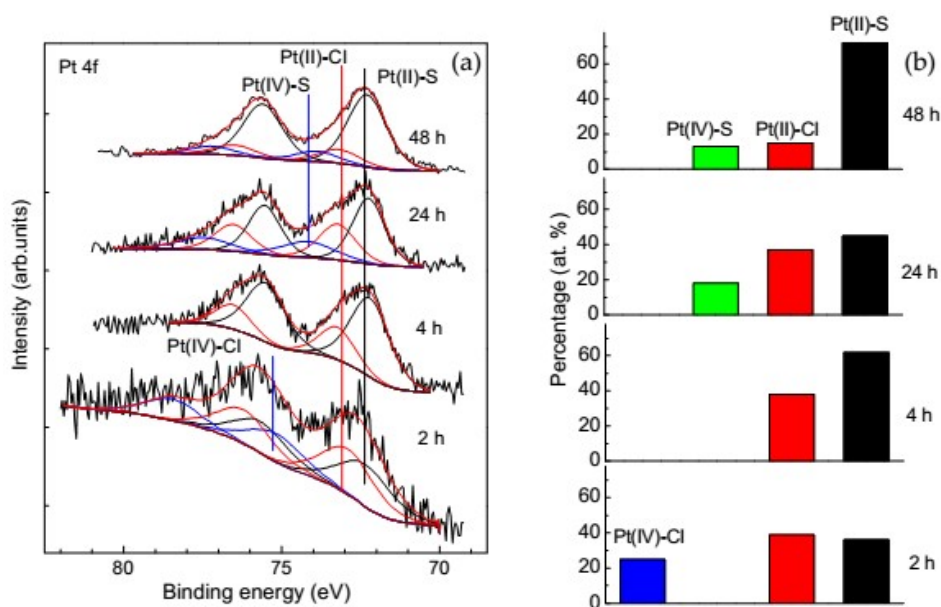


**Figure 6.** (a) Normalized Pt 4f spectra of pyrrhotite treated with 1 mmol/L H<sub>2</sub>PtCl<sub>6</sub> solution for 2 h, 4 h, 24 h and 48 h, and (b) distribution of the surface Pt species.

### 3.3.3. Change of Platinum Species in the Deposition Process on Pyrrhotite

About 80% of Pt immobilized on the pyrrhotite surface (Figure 7) is represented by divalent Pt bound to Cl and S, with the former being dominant for short deposition (e.g., 60% vs. 22% after 2 h), and the latter increasing with time and prevailing after 24 h reaction (36% vs. 40%). The amount of Pt(IV) tends to decrease within the range of 30% to 20% with increasing the interaction time. Concurrently, the component at 75.2 eV shifts towards 74.1 eV, suggesting that the Pt(IV)-Cl adsorbates transform to Pt(IV)-S species.

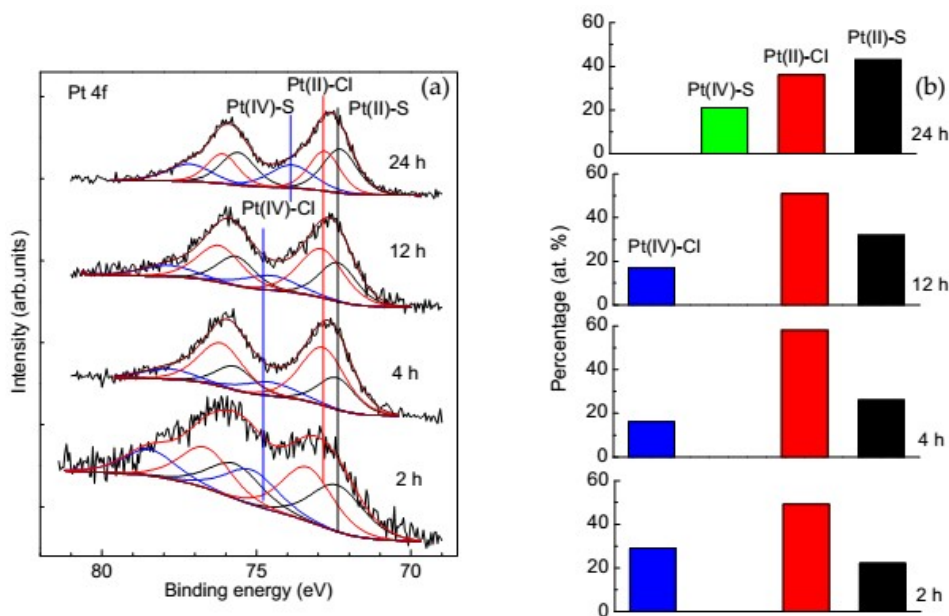


**Figure 7.** (a) Normalized Pt 4f spectra for pyrrhotite samples after 2, 4, 12 and 24 h of the interaction with 1 mmol/L H<sub>2</sub>PtCl<sub>6</sub> solution, and (b) corresponding distribution of the Pt species.

Both the reduction and sulfidization of immobilized Pt(IV)–Cl species are faster on pyrrhotite than pyrrhotite, despite pyrite being much more chemically inert. At the same time, it should be taken in mind that the total uptake of Pt is somewhat higher at pyrrhotite.

### 3.4. Influence of the Preliminary Modification of the Mineral Surface on the Platinum Deposition

One can expect that the state of a mineral surface is modified, for example, the weathering and mineral processing could affect the interaction with Pt-bearing solutions. The preliminary oxidative leaching of pyrrhotite in the 0.25 M FeCl<sub>3</sub> + HCl solution (30 min at 50 °C) leads to a significant increase in the amount of the deposited Pt (Figure 8a). The pre-treatment in 1 M HCl under the non-oxidative dissolution conditions (−50 mV, 10 min), which produces a massive metal-deficient layer on the pyrrhotite surface [44], also results in an increased amount of Pt on the surface but to a smaller extent than after the oxidative treatment (Figure 8). After the anodic pre-oxidation at 0.5 V (region of potentials of the passive dissolution of pyrrhotite) a significant decrease in the Pt deposition, with Pt/S being two times lower as compared to unreacted pyrrhotite is observed.

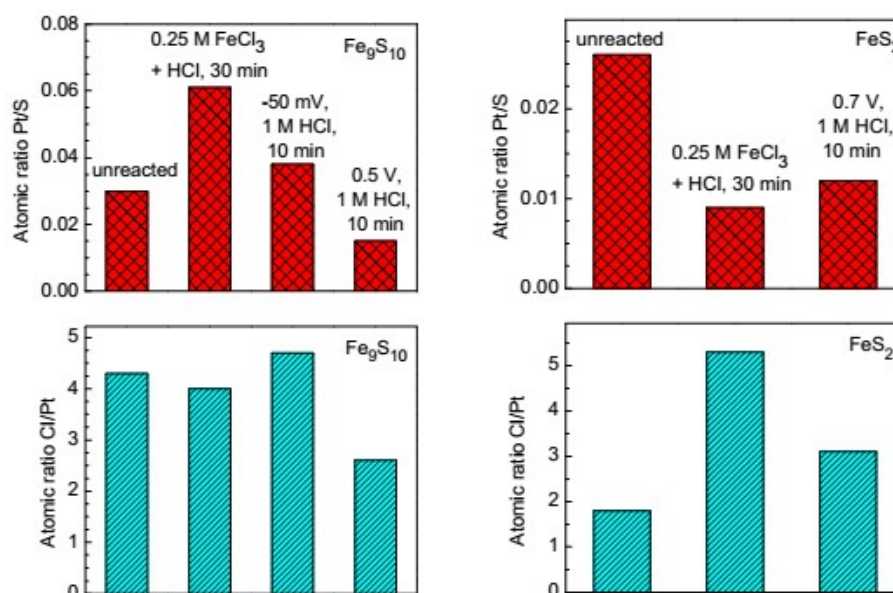


**Figure 8.** Pt/S and Pt/Cl atomic ratios for pyrrhotite (left panels) and pyrite (right panels) after various chemical pre-treatment followed by 2 h interaction with 1 mmol/L H<sub>2</sub>PtCl<sub>6</sub> solution.

Figure 9 shows the Pt 4f spectra and forms of Pt deposited on the preliminarily oxidized pyrrhotite; the Pt concentration on the oxidized pyrite is low, so the spectra were of poor quality and are not shown here. On the base of these data, we hypothesize that the enhanced uptake of Pt at pyrrhotite mainly as the sulfide species is due to excessive S in the Fe-depleted surface layers produced by the chemical pre-treatment [44,45]. The Fe depletion and S enrichment of the reacted pyrite are much lower [44], and the oxidation promotes mainly increasing surface concentration of adsorbed chloride ions, which probably retard the adsorption of the Pt complex ions.

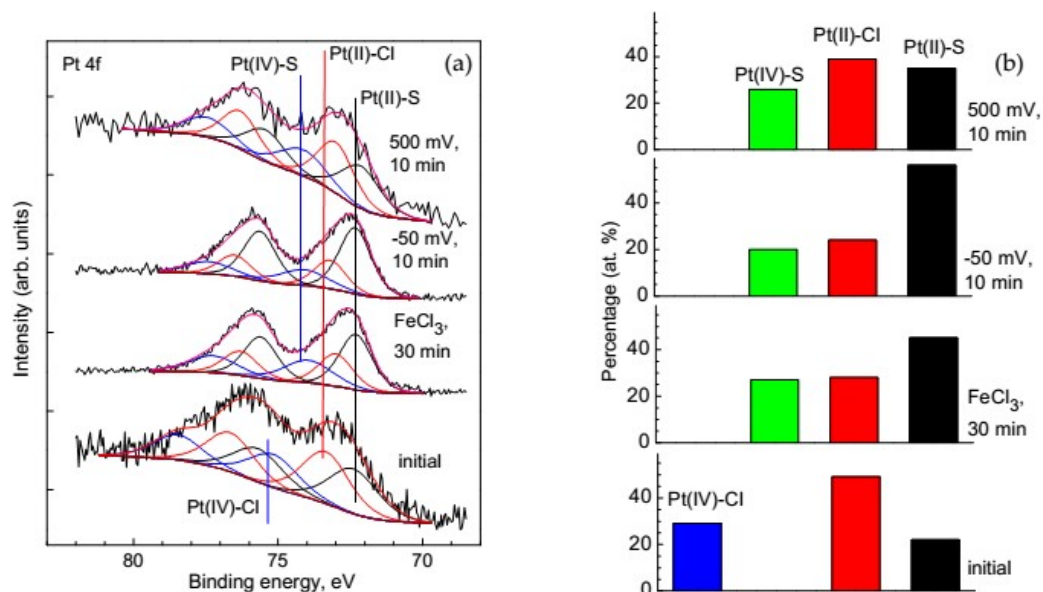


**Figure 9.** (a) Normalized XPS Pt 4f spectra of pyrrhotite after the deposition of Pt from 1 mmol/L H<sub>2</sub>PtCl<sub>6</sub> solution onto unreacted surface and onto the surface preliminarily treated in 0.25 mol/L FeCl<sub>3</sub> + HCl during 30 min, 1 mol/L HCl at the potential of −50 mV, and at the potential of 500 mV (10 min), and (b) corresponding diagram of the distribution of the Pt forms.

### 3.5. Platinum Species on Different Sulfide Minerals

In the Pt 4f spectra of galena (Figure 10) two distinct components are shown one with the binding energy of 72.3 eV and contribution of 65%, and another at 73.4 eV amounting of 35%, almost independent of the deposition time. The first component corresponds to Pt(II)-S species, and the second originates from Pt(II) atoms bound to Cl<sup>−</sup>, apparently in adsorbed PtCl<sub>4</sub><sup>2−</sup> ions. Neither tetravalent Pt nor metallic Pt were observed on galena under the given conditions.

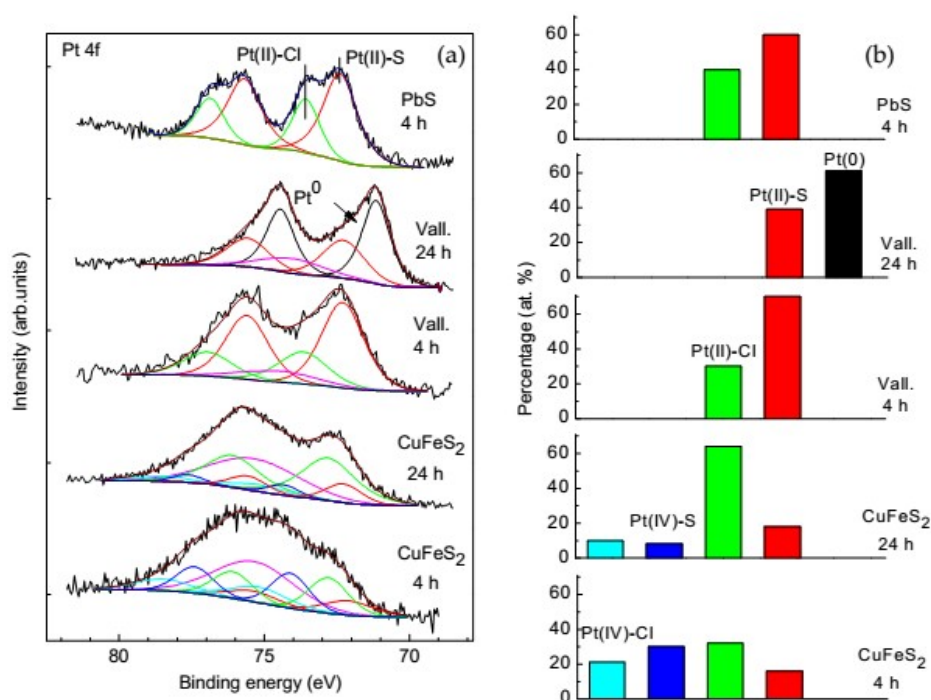


**Figure 10.** (a) XPS Pt 4f spectra of the sulfide minerals reacted with 1 mmol/L H<sub>2</sub>PtCl<sub>6</sub> solution and (b) corresponding distribution diagrams of the platinum forms.

The spectra of Pt collected from valleriite after 4 h of interaction with the  $\text{H}_2\text{PtCl}_6$  solution are rather similar to galena, with the two doublets being somewhat wider and contribution of the chloride complex being lower. Surprisingly, metallic Pt of ~60% from the entire amount of Pt, is found to form on valleriite as the reaction progresses, which is evidenced by the appearance of the Pt  $4f_{7/2}$  peak at 71.5 eV. The remainder is Pt(II) bound with sulfur (the binding energy of 72.3 eV), while contributions of Pt–Cl species is lower. Noteworthy, the Pt 4f bands are overlapped with Cu 3p band at ~75 eV, which is weak for valleriite. Chalcopyrite, has almost the same composition as sulfide nanolayers in valleriite, but the uptake of Pt is much lower, with Pt–Cl species dominating and Pt(IV) species notably contributing especially in the initial stages; rather intense Cu 3p line overlaps the Pt 4f spectra, making difficult their unanimous fitting.

#### 4. Discussion

The process of Pt immobilization onto sulfide minerals appears to proceed via a sequence of stages. The first is the adsorption of Pt-chloride complexes. The following stages include the substitution of chloride ions with sulfide (and, maybe, di- and polysulfide) anions and reduction of tetravalent Pt to divalent Pt, and to metallic state in the case of valleriite. It is possible that there exist more Pt products in addition to those described above, including intermediates of the substitution reactions, involving some  $\text{OH}^-$  or/and  $\text{H}_2\text{O}$  ligands, etc. However, exact compositions of the Pt species cannot be unequivocally derived from the above XPS data because of contributions of numerous surface S-, Cl-, O-bearing entities at the sulfide substrates and errors of the fitting procedures.

As it was demonstrated for pyrrhotite and pyrite, the total and relative contents of Pt products differ as a function not only of the reaction time but also of mineral nature, the state of its surface, in particular, a measure of oxidation and composition of the modified metal sulfide. The key factor seems to be the activity of the surface sulfur anions involved in the reduction of Pt(IV) and the substitution of  $\text{Cl}^-$  ions in the coordination sphere of Pt. In a number of cases, e.g., for galena and pyrrhotite, Pt complexes may be reduced by aqueous bisulfide ions (hydrogen sulfide) formed due to acidic dissolution of the metal sulfides. Both these effects are related with reactivity of metal sulfide minerals, which is commonly known to increase in the order pyrite < chalcopyrite < valleriite < galena, pyrrhotite, that generally agrees with increasing the uptake of Pt (Figure 5). Furthermore, oxidation of pyrrhotite, including in ambient air, results in its passivation [54–56], while both non-oxidative and oxidative preliminary leaching causes the formation of more active over-stoichiometric sulfide, di- and polysulfide anions, which facilitate the fixation of Pt via the reduction and sulfidization reaction.

The formation of Pt(IV)–S species in the next stages can be explained by oxidation of the Pt(II)–S by di- and polysulfide groups as reported in refs [57,58]. The oxidative capability of the –S–S– species arising at the sulfide mineral surfaces upon their prolonged oxidation seems to be in fact mediated by Fe(III) entities and oxygen.

The largest uptake of Pt was observed at valleriite, the most important mineral of so-called “coppery” ores of the Noril’sk deposits (about 7% of the total resources), which form veins in sedimentary and metamorphic rocks on the margins of the massive magmatic ores and is known for increased contents of PGEs [59,60]. Valleriite is a sulfide-hydroxide composite mineral where the sulfide nanolayers with the composition  $\text{CuFeS}_n$  close to chalcopyrite alternate with brucite-like hydroxide nanolayers  $[\text{Mg},\text{Al}(\text{OH})_2]$  [61–63]. The hydroxide layers are believed to have positive charge due to the substitution of  $\text{Mg}^{2+}$  for  $\text{Al}^{3+}$ , and so the sulfide nanolayers are negative to support electro neutrality [54], but this has not been confirmed experimentally yet. We believe that the localization of electron density at the sulfide layers makes them a strong reducing agent, which is capable of transforming Pt compounds to the metallic state over its immobilization. This mechanism corroborates with the fact that chalcopyrite being the structural analogue of the sulfide nanolayers and a precursor of valleriite in the geochemical processes, exhibits much weaker reducing properties towards Pt(II,IV) species.

## 5. Conclusions

1. The interaction of the aqueous solutions of  $\text{H}_2\text{PtCl}_6$  with the surface of sulfide minerals results in the deposition of Pt on their surface. The amount of the deposited Pt increases with time.
2. The highest rate of Pt uptake is observed on galena and valleriite.
3. The preliminary moderate oxidation and non-oxidative leaching of pyrrhotite creating metal-deficient surface layers usually promotes Pt deposition. In the case of pyrite, the preliminary oxidation decreases the amount of the deposited Pt.
4. The main Pt phases immobilized on sulfide minerals are sulfides and chloride complexes of Pt(II), and, to a smaller extent, chloride complexes of tetravalent Pt; no Pt(IV) was observed on galena and valleriite. As the reaction progresses, the amount of Pt(IV) usually decreases while the amount of the sulfide forms increases.
5. Metallic Pt was found to form only on valleriite, probably owing to the negative charge localized at sulfidic nanolayers.
6. The di- and polysulfide surface species arising on sulfide minerals upon their oxidation are capable of oxidizing immobilized Pt(II)–S to Pt(IV)–S species.

**Supplementary Materials:** The following are available online at <http://www.mdpi.com/2075-163X/8/12/578/s1>, Figure S1: XPS the S 2p spectra from a droplet of sol formed in the reaction  $\text{H}_2\text{PtCl}_6 + \text{H}_2\text{S}$  dried on pyrolytic graphite, Figure S2: SR photoelectron Pt 4f spectra of the surfaces of pyrrhotite (a) and pyrite (b) after the interaction with solution of 1 mmol/L  $\text{H}_2\text{PtCl}_6 + 0.03$  mol/L HCl for 12 h. Table S1: Atomic concentrations of the elements on the surfaces of different sulfide minerals after 2 h interaction with 1 mmol/L  $\text{H}_2\text{PtCl}_6$ .

**Author Contributions:** A.R. and Y.M. conceived and designed the study; A.R. prepared samples for all experiments; M.L. performed synthetic, AFM experiments; A.R. and Y.M. conducted XPS measurements; A.R. and Y.M. wrote the paper.

**Funding:** This research was funded by Russian Foundation for Basic Research and the Government of Krasnoyarsk Territory, Krasnoyarsk Regional Fund of Science to the research project: The investigation of interaction aqueous solutions of gold, platinum and palladium sulfide nano- and mesoscale particles with sulfide and oxide minerals, project number 17-45-240759.

**Conflicts of Interest:** The authors declare no conflict of interest. The funding sponsors had no role in the design of the study; in the collection, analyses, or interpretation of data; in the writing of the manuscript, and in the decision to publish the results.

## References

1. Dey, S.; Jain Vimal, K. Platinum Group Metal Chalcogenides: Their syntheses and applications in catalysis and materials science. *Platin. Metals Rev.* **2004**, *48*, 16–29.
2. Chia, X.; Adriano, A.; Lazar, P.; Sofer, Z.; Luxa, J.; Pumera, M. Layered platinum dichalcogenides ( $\text{PtS}_2$ ,  $\text{PtSe}_2$ , and  $\text{PtTe}_2$ ) electrocatalysis: Monotonic dependence on the chalcogen size. *Adv. Funct. Mater.* **2016**, *26*, 4306–4318. [[CrossRef](#)]
3. Bhatt, R.; Bhattacharya, S.; Basu, R. Growth of  $\text{Pd}_4\text{S}$ , PdS and  $\text{PdS}_2$  films by controlled sulfurization of sputtered Pd on native oxide of Si. *Thin Solid Films* **2013**, *539*, 41–46. [[CrossRef](#)]
4. Jha, M.K.; Lee, J.; Kim, M.; Jeong, J.; Kim, B.; Kumar, V. Hydrometallurgical recovery/recycling of platinum by the leaching of spent catalysts: A review. *Hydrometallurgy* **2013**, *133*, 23–32. [[CrossRef](#)]
5. Junge, M.; Oberthür, T.; Kraemer, D.; Melcher, F.; Pina, R.; Derrey, I.T.; Manyeruke, T.; Strauss, H. Distribution of platinum-group elements in pristine and near-surface oxidized Platreef ore and the variation along strike, northern Bushveld Complex, South Africa. *Miner. Depos.* **2018**. [[CrossRef](#)]
6. Kraemer, D.; Junge, M.; Oberthür, T.; Bau, M. Improving recoveries of platinum and palladium from oxidized Platinum-Group Element ores of the Great Dyke, Zimbabwe, using the biogenic siderophore Desferrioxamine B. *Hydrometallurgy* **2015**, *152*, 169–177. [[CrossRef](#)]
7. Kraemer, D.; Junge, M.; Oberthür, T.; Bau, M. Oxidized ores as future resource for platinum group metals: Current state of research. *Chem. Ing. Tech.* **2017**, *89*, 53–63. [[CrossRef](#)]
8. Gammons, C.H.; Bloom, M.S.; Yu, Y. Experimental investigation of the hydrothermal geochemistry of platinum and palladium: I. Solubility of platinum and palladium sulfide minerals in  $\text{NaCl}/\text{H}_2\text{SO}_4$  solutions at 300 °C. *Geochim. Cosmochim. Acta* **1992**, *56*, 3881–3894. [[CrossRef](#)]

9. McDonald, I.; Ohnenstetter, D.; Rowe, J.P.; Tredoux, M.; Pattrick, R.A.D.; Vaughan, D.J. Platinum precipitation in the Waterberg deposit, Naboomspruit, South Africa. *S. Afr. J. Geol.* **1999**, *102*, 184–191.
10. Oberthür, T.; Melcher, F.; Fusswinkel, T.; van den Kerkhof, A.M.; Sosa, G.M. The hydrothermal Waterberg platinum deposit, Mookgophong (Naboomspruit), South Africa. Part 1: Geochemistry and ore mineralogy. *Mineral. Mag.* **2018**, *82*, 725–749. [[CrossRef](#)]
11. Gammons, C.H.; Bloom, M.S. Experimental investigation of the hydrothermal geochemistry of platinum and palladium: II. The solubility of PtS and PdS in aqueous sulfide solutions to 300 °C. *Geochim. Cosmochim. Acta* **1992**, *57*, 2451–2467. [[CrossRef](#)]
12. Mountain, B.W.; Wood, S.A. Chemical controls on the solubility, transport, and deposition of platinum and palladium in hydrothermal solutions: A thermodynamic approach. *Econ. Geol.* **1988**, *83*, 492–510. [[CrossRef](#)]
13. Gammons, C.H. Experimental investigations of the hydrothermal geochemistry of platinum and palladium: V. Equilibria between platinum metal, Pt(II), and Pt (IV) chloride complexes at 25 to 300 °C. *Geochim. Cosmochim. Acta* **1992**, *59*, 1655–1667. [[CrossRef](#)]
14. Gammons, C.H. Experimental investigation of the hydrothermal geochemistry of platinum and palladium: IV. The stoichiometry of Pt (IV) and Pd (II) chloride complexes at 100 to 300 °C. *Geochim. Cosmochim. Acta* **1994**, *59*, 3881–3894. [[CrossRef](#)]
15. Godel, B.; Barnes, S.-J. Platinum-group elements in sulfide minerals and the whole rocks of the JM Reef (Stillwater Complex): Implication for the formation of the reef. *Chem. Geol.* **2008**, *248*, 272–294. [[CrossRef](#)]
16. Hyland, M.M.; Bancroft, G.M. Palladium sorption and reduction on sulphide mineral surfaces: An XPS and AES study. *Geochim. Cosmochim. Acta* **1989**, *54*, 117–130. [[CrossRef](#)]
17. Plyusnina, L.P.; Likhoidov, G.G.; Shcheka, Z.A. Experimental modeling of platinum behavior under hydrothermal conditions (300–500 °C and 1 kbar). *Geochem. Int.* **2007**, *45*, 1124–1130. [[CrossRef](#)]
18. Wood, S.A.; Mountain, B.W.; Pan, P. The aqueous geochemistry of platinum, palladium and gold: Recent experimental constraints and a re-evaluation of theoretical prediction. *Can. Mineral.* **1992**, *30*, 955–982.
19. Jaireth, S. The calculated solubility of platinum and gold in oxygen-saturated fluids and the genesis of platinum-palladium and gold mineralization in the unconformity-related uranium deposits. *Miner. Depos.* **1992**, *27*, 42–54. [[CrossRef](#)]
20. Watkinson, D.H.; Melling, D.R. Hydrothermal origin of platinum-group mineralization in low-temperature copper sulfide-rich assemblages, Salt Chuck Intrusion, Alaska. *Econ. Geol.* **1992**, *87*, 175–184. [[CrossRef](#)]
21. Reith, F.; Zammit, C.M.; Shar, S.S.; Etschmann, B.; Bottrill, R.; Southam, G.; Ta, C.; Kilburn, M.; Oberthür, T.; Ball, A.S.; et al. Biological role in the transformation of platinum-group mineral grains. *Nat. Geosci.* **2016**, *9*, 1–6. [[CrossRef](#)]
22. Reith, O.F.; Campbell, S.G.; Ball, A.S.; Pring, A.; Southam, G. Platinum in Earth surface environments. *Earth-Sci. Rev.* **2014**, *131*, 1–21. [[CrossRef](#)]
23. Pawlak, J.; Łodyga-Chruścińska, E.; Chrustowicz, J. Fate of platinum metals in the environment. *J. Trace Elem. Med. Biol.* **2014**, *28*, 247–254. [[CrossRef](#)] [[PubMed](#)]
24. Reith, F.; Shuster, J. *Geomicrobiology and Biogeochemistry of Precious Metals*; MDPI: Basel, Switzerland, 2018; pp. 114–131; ISBN 978-3-03897-347-8.
25. Piña, R.; Gervilla, F.; Barnes, S.-J.; Oberthür, T.; Lunar, R. Platinum-group element concentrations in pyrite from the Main Sulfide Zone of the Great Dyke of Zimbabwe. *Miner. Depos.* **2016**, *51*, 853–872. [[CrossRef](#)]
26. Dare, S.A.S.; Barnes, S.-J.; Prichard, H.M.; Fisher, P.C. Chalcophile and platinum-group element (PGE) concentrations in the sulfide minerals from the McCreedy East deposit, Sudbury, Canada, and the origin of PGE in pyrite. *Miner. Depos.* **2011**, *46*, 381–407. [[CrossRef](#)]
27. Junge, M.; Wirth, R.; Oberthür, T.; Melcher, F.; Schreiber, A. Mineralogical siting of platinum-group elements in pentlandite from the Bushveld Complex, South Africa. *Miner. Depos.* **2015**, *50*, 41–54. [[CrossRef](#)]
28. Kubrakova, I.V.; Tyutyunnik, O.A.; Koshcheeva, I.Y.; Sadagov, A.Y.; Nabiullina, S.N. Migration behavior of platinum group elements in natural and technogeneuous systems. *Geochem. Int.* **2017**, *55*, 108–124. [[CrossRef](#)]
29. Torres, R.; Lapidus, G.T. Platinum, palladium and gold leaching from magnetite ore, with concentrated chloride solutions and ozone. *Hydrometallurgy* **2016**, *166*, 185–194. [[CrossRef](#)]
30. Fuchs, W.A.; Rose, A.W. The geochemical behavior of platinum and palladium in the weathering cycle in the Stillwater complex, Montana. *Econ. Geol.* **1974**, *69*, 332–346. [[CrossRef](#)]
31. Adams, M.; Liddell, K.; Holohan, T. Hydrometallurgical processing of Platreef flotation concentrate. *Miner. Eng.* **2011**, *24*, 545–550. [[CrossRef](#)]

32. Liddell, K.S.; Adams, M.D. Kell hydrometallurgical process for extraction of platinum group metals and base metals from flotation concentrates. *J. S. Afr. Inst. Min. Metall.* **2012**, *112*, 31–36.
33. Liddell, K.; Newton, T.; Adams, M.; Muller, B. Energy consumption for Kell hydrometallurgical refining versus conventional pyrometallurgical smelting and refining of PGM concentrates. *J. S. Afr. Inst. Min. Metall.* **2011**, *111*, 127–132.
34. Mpinga, C.N.; Eksteen, J.J.; Aldrich, C.; Dyer, L. Direct leach approaches to Platinum Group Metal (PGM) ores and concentrates: A review. *Miner. Eng.* **2015**, *78*, 93–113. [[CrossRef](#)]
35. Mwase, J.M.; Petersen, J.; Eksteen, J.J. A conceptual flowsheet for heap leaching of platinum group metals (PGMs) from a low-grade ore concentrate. *Hydrometallurgy* **2012**, *111*, 129–135. [[CrossRef](#)]
36. Mwase, J.M.; Petersen, J.; Eksteen, J.J. Assessing a two-stage heap leaching process for Platreef flotation concentrate. *Hydrometallurgy* **2012**, *129*, 74–81. [[CrossRef](#)]
37. Mwase, J.M.; Petersen, J.; Eksteen, J.J. A novel sequential heap leach process for treating crushed Platreef ore. *Hydrometallurgy* **2014**, *141*, 97–104. [[CrossRef](#)]
38. Mikhlin, Y.L.; Romanchenko, A.S. Gold deposition on pyrite and the common sulfide minerals: An STM/STS and SR-XPS study of surface reactions and Au nanoparticles. *Geochim. Cosmochim. Acta* **2007**, *71*, 5985–6001. [[CrossRef](#)]
39. Mikhlin, Y.L.; Romanchenko, A.S.; Likhatski, M.N.; Karacharov, A.; Erenberg, S.B.; Trubina, S.V. Understanding the initial stages of precious metals precipitation: Nanoscale metallic and sulfidic species of gold and silver on pyrite surfaces. *Ore Geol. Rev.* **2011**, *42*, 47–54. [[CrossRef](#)]
40. Mycroft, J.R.; Bancroft, G.M.; McIntyre, N.S.; Lorimer, J.W. Spontaneous deposition of gold on pyrite from solutions containing Au (III) and Au (I) chlorides. Part I: A surface study. *J. Electroanal. Chem.* **1990**, *292*, 139–152. [[CrossRef](#)]
41. Romanchenko, A.S.; Mikhlin, Y.L. An XPS study of products formed on pyrite and pyrrhotite by reacting with palladium(II) chloride solutions. *J. Struct. Chem.* **2015**, *56*, 531–537. [[CrossRef](#)]
42. Gulyaev, R.V.; Stadnichenko, A.I.; Slavinskaya, E.M.; Koscheev, S.V.; Ivanova, A.S.; Boronin, A.I. In situ preparation and investigation of Pd/CeO<sub>2</sub> catalysts for the low-temperature oxidation of CO. *Appl. Catal. A Gen.* **2012**, *439*, 41–50. [[CrossRef](#)]
43. Kibis, L.S.; Stadnichenko, A.I.; Koscheev, S.V.; Zaikovskii, V.I.; Boronin, A.I. Highly oxidized palladium nanoparticles comprising Pd<sup>4+</sup> species: Spectroscopic and structural aspects, thermal stability, and reactivity. *J. Phys. Chem. C* **2012**, *116*, 19342–19348. [[CrossRef](#)]
44. Mikhlin, Y.L.; Tomashevich, Y.V.; Pashkov, G.L.; Okotrub, A.V.; Asanov, I.P.; Mazalov, L.N. Electronic structure of the non-equilibrium iron-deficient layer of hexagonal pyrrhotite. *Appl. Surf. Sci.* **1998**, *125*, 73–84. [[CrossRef](#)]
45. Mikhlin, Y. Reactivity of pyrrhotite surfaces: An electrochemical study. *Phys. Chem. Chem. Phys.* **2000**, *2*, 5672–5677. [[CrossRef](#)]
46. Mikhlin, Y.; Romanchenko, A.; Shagaev, A. Scanning probe microscopy studies of PbS surfaces oxidized in air and etched in aqueous acid solutions. *Appl. Surf. Sci.* **2006**, *252*, 5245–5258. [[CrossRef](#)]
47. Mikhlin, Y.; Kuklinskiy, A.; Mikhlina, E.; Kargin, V.; Asanov, I. Electrochemical behaviour of galena (PbS) in aqueous nitric acid and perchloric acid solutions. *J. Appl. Electrochem.* **2004**, *34*, 37–46. [[CrossRef](#)]
48. Mikhlin, Y.L.; Tomashevich, Y.V.; Asanov, I.P.; Okotrub, A.V.; Varnek, V.A.; Vyalikh, D.V. Spectroscopic and electrochemical characterization of the surface layers of chalcopyrite (CuFeS<sub>2</sub>) reacted in acidic solutions. *Appl. Surf. Sci.* **2004**, *225*, 395–409. [[CrossRef](#)]
49. Mikhlin, Y.L.; Romanchenko, A.S.; Tomashevich, E.V.; Volochaev, M.N.; Laptev, Y.V. XPS and XANES study of layered mineral valleriite. *J. Struct. Chem.* **2017**, *58*, 1137–1143. [[CrossRef](#)]
50. Laptev, Y.V.; Shevchenko, V.S.; Urakaev, F.K. Sulphidation of valleriite in SO<sub>2</sub> solutions. *Hydrometallurgy* **2009**, *98*, 201–205. [[CrossRef](#)]
51. Muhler, M.; Paal, Z. Sulfided platinum black by XPS. *Surf. Sci. Spectra* **1996**, *4*, 125–129. [[CrossRef](#)]
52. Dembowski, J.; Marosi, L.; Essig, M. Platinum disulfide by XPS. *Surf. Sci. Spectra* **1994**, *2*, 133–137. [[CrossRef](#)]
53. Karhu, H.; Kalantar, A.; Väyrynen, I.J.; Salmi, T.; Murzin, D.Y. XPS analysis of chlorine residues in supported Pt and Pd catalysts with low metal loading. *Appl. Catal. A* **2003**, *247*, 283–294. [[CrossRef](#)]
54. Mikhlin, Y.; Tomashevich, Y.; Vorobyev, S.; Saikova, S.; Romanchenko, A.; Félix, R. Hard X-ray photoelectron and X-ray absorption spectroscopy characterization of oxidized surfaces of iron sulfides. *Appl. Surf. Sci.* **2016**, *387*, 796–804. [[CrossRef](#)]

55. Mikhlin, Y.; Nasluzov, V.; Romanchenko, A.; Tomashevich, Y.; Shor, A.; Félix, R. Layered structure of the near-surface region of oxidized chalcopyrite ( $\text{CuFeS}_2$ ): Hard X-ray photoelectron spectroscopy, X-ray absorption spectroscopy and DFT+U studies. *Phys. Chem. Chem. Phys.* **2017**, *19*, 2749–2759. [[CrossRef](#)] [[PubMed](#)]
56. Mikhlin, Y.; Romanchenko, A.; Tomashevich, Y.; Shurupov, V. Near-surface regions of electrochemically polarized chalcopyrite ( $\text{CuFeS}_2$ ) as studied using XPS and XANES. *Phys. Procedia* **2016**, *84*, 390–396. [[CrossRef](#)]
57. Bonnington, K.J.; Jennings, M.C.; Puddephatt, R.J. Oxidative addition of S-S bonds to dimethylplatinum(II) complexes: Evidence for a binuclear mechanism. *Organometallics* **2008**, *27*, 6521–6530. [[CrossRef](#)]
58. McCready, M.S.; Puddephatt, R.J. Oxidative addition of functional disulfides to platinum(II): Formation of chelating and bridging thiolate–carboxylate complexes of platinum(IV). *Inorg. Chem. Commun.* **2011**, *14*, 210–212. [[CrossRef](#)]
59. Yakubchuk, A.; Nikishin, A. Noril'sk-Talnakh Cu-Ni-PGE deposits: A revised tectonic model. *Miner. Depos.* **2004**, *39*, 125–142. [[CrossRef](#)]
60. Harris, D.C.; Cabry, L.J.; Stewart, J.M. A “valleriite-type” mineral from Noril'sk, Western Siberia. *Am. Mineral.* **1970**, *55*, 2110–2114.
61. Evans, H.T.; Allman, R. The crystal structure and crystal chemistry of valleriite. *Zeitschrift für Kristallographie* **1968**, *127*, 73–93. [[CrossRef](#)]
62. Hughes, A.E.; Kakos, G.A.; Turney, T.W.; Williams, T.B. Synthesis and structure of valleriite, a layered Metal Hydroxide/Sulfide Composite. *J. Solid State Chem.* **1993**, *104*, 422–436. [[CrossRef](#)]
63. Li, R.; Cui, L. Investigations on valleriite from Western China: Crystal chemistry and separation properties. *Int. J. Miner. Process.* **1994**, *41*, 271–283. [[CrossRef](#)]



© 2018 by the authors. Licensee MDPI, Basel, Switzerland. This article is an open access article distributed under the terms and conditions of the Creative Commons Attribution (CC BY) license (<http://creativecommons.org/licenses/by/4.0/>).